Monte Carlo Simulations of a Coarse Grain Model for Block Copolymers and Nanocomposites

François A. Detcheverry,[†] Huiman Kang,[†] Kostas Ch. Daoulas,[‡] Marcus Müller,[‡] Paul F. Nealey,[†] and Juan J. de Pablo*,[†]

Department of Chemical and Biological Engineering, University of Wisconsin−Madison, Madison, Wisconsin 53706-1691, and Institut für Theoretische Physik, Georg-August Universität, 37077 Göttingen, Germany

Received November 12, 2007; Revised Manuscript Received March 14, 2008

ABSTRACT: A coarse grain model and a Monte Carlo sampling formalism are proposed for simulations of self-assembly in block copolymer melts and nanoparticle−copolymer composites. Our approach relies on a particle-based representation of the system, it does not invoke a saddle point approximation, and it permits treatment of large three-dimensional systems. We provide a detailed description of the model and methods and discuss their relationship to results from self-consistent-field theory and single chain in mean field simulations. The validity of the proposed approach is addressed by applying it to study systems whose description within existing approaches would be demanding. In particular, we use it to examine the directed assembly of copolymer blends and nanoparticles on nanopatterned substrates. We show that results from simulations are in good agreement with experiment, and we use our theoretical findings to help explain the experimental observations.

I. Introduction

Much of our current understanding of block copolymers has emerged from self-consistent-field theoretic studies. The phase behavior and thermodynamic properties of a wide variety of systems have now been determined:[1] starting from relatively simple cases, such as symmetric diblock copolymers, fundamental and applied considerations have fueled an emerging interest in increasingly complex systems, including multiblock copolymers, materials having different architectures (e.g., star polymers), and multicomponent blends. Despite its many successes, however, the self-consistent-field theory (SCFT) exhibits certain limitations that, if overcome, would permit study of a number of materials and circumstances that have not been considered in the past. While sophisticated numerical schemes have been developed over the past several years, solution of the SCFT equations remains computationally demanding. Several SCFT studies have now considered select three-dimensional block copolymer systems (an example is given in ref 2), but a majority of the published SCFT calculations has been limited to two-dimensional systems. Fully three-dimensional calculations over large domains are still challenging, and it continues to be difficult to address a number of questions of fundamental and practical interest that are intrinsically three-dimensional. Examples include the bicontinuous morphologies or the directed assembly of thin films by patterned substrates. SCFT involves a saddle point (or mean field) approximation that neglects all composition fluctuations. While this approximation is justified in many situations of interest (including melts or concentrated solutions of high molecular weight), there are also systems for which it poses limitations, including diblock copolymers or blends close to an order−disorder transition, dilute polymer solutions, and polyelectrolytes. Moving beyond the saddle point approximation requires the use of field-theoretic methods that are just now being developed,[3] and the computational demands of emerging approaches are such that only a small number of situations have been considered.[4−6] Perhaps more importantly, past efforts aimed at extending traditional SCFT approaches to describe the interplay of particular block copolymer morphologies with nonpolymeric objects (such as nanoscale fillers) have met with limited success.

Several alternative approaches have been explored to overcome the limitations of SCFT. These include many-body Monte Carlo simulations and single chain in mean field (SCMF) simulations. In many-body simulations,[7,8] the polymer subunits (atoms, monomers, or beads) interact through an explicit potential, usually pairwise additive, such as the Lennard-Jones potential, and all coordinates are explicit degrees of freedom. In SCMF simulations,[9] the starting point is a coarse grain description of the polymeric melt analogous to that employed in SCFT. The method, however, is particle-based and can therefore describe chain conformations explicitly. In contrast to SCFT, SCMF simulations do not rely on a saddle point approximation and can include some fluctuation effects such as the correlation hole in a dense melt or the first-order nature of the order−disorder transition in a symmetric diblock copolymer.[10] The SCMF simulation approach permits study of relatively large, three-dimensional systems. An example is provided by recent calculations in which a lamellae-forming blend deposited on a two-dimensional chemically patterned substrate was shown to form a bicontinuous phase.[11] Another attractive feature of SCMF simulations is the ability to describe the dynamics with different assumptions than those involved in dynamic versions of SCFT; recent SCMF simulation studies have considered the spinodal decomposition of a symmetric binary blend and the kinetics of solvent evaporation in a thin film.[12]

In spite of its advantages, SCMF simulations are not without shortcomings. While in SCFT the fields are static quantities that describe the average interaction between a chain and its neighbors, the fields in SCMF simulations describe the instantaneous interactions and therefore evolve in time. It is important to emphasize, however, that those fields remain approximate because, on short time scales, they are decoupled from the actual molecules. The accuracy of this "quasi-instantaneous field approximation" is controlled by the choice of several discretization parameters. In principle, it is always possible to chose those parameters so as to reach a given accuracy; if the local structure on the scale of a monomer is to be resolved, this may

* To whom correspondence should be addressed.
[†] University of Wisconsin−Madison.
[‡] Georg-August Universität.

10.1021/ma702514v CCC: $40.75
Published on Web 06/11/2008

imply large computation times. Perhaps more importantly, extensions of the SCMF simulation approach to mixtures of polymer and nonpolymeric objects have not been attempted so far. For such systems, keeping the quasi-instantaneous field approximation at a reasonable level of accuracy would be challenging.

It is therefore desirable to develop a method that would avoid the saddle point approximation of SCFT as well as the "quasi-instantaneous field approximation" of SCMF simulations, while at the same time remaining faster than a many-body Monte Carlo simulation. Such a method should be capable of describing complex three-dimensional geometries and nanocomposite blends.

The approach proposed in this work relies on Monte Carlo (MC) simulations of a coarse grain model. Coarse grain MC simulations (as they will be referred to in the remainder of this work) were originally introduced in the context of brushes[13–15] but have been only briefly considered in the context of ordered diblock copolymer melts.[10] As shown in what follows, our coarse grain MC simulation approach has a broad range of applicability for study of block copolymer systems and is capable of describing the effects of patterned substrates, complex geometries, and nanoscale inclusions with relatively modest computational efforts.

In order to establish both the validity and the range of applicability of our proposed approach, two types of system are considered in this work. The first consists of a high molecular weight block copolymer melt, for which results from a variety of computational approaches can be found in the literature. The second system is a mixture of polymeric and nonpolymeric objects. For concreteness, we focus on the particular case of nanoparticles dispersed in a copolymer, which has attracted considerable attention in recent years, both experimentally and theoretically.[16] In order to place a stringent test on the predictive capability of our proposed approach, we consider the particular case of a mixture deposited on a patterned substrate, for which particularly insightful experimental results have just become available.

In order to better grasp the behaviors that a theory for polymer nanocomposites must capture, it is instructive to briefly discuss some of the various types of applications that are currently being sought. The first consist of dispersing nanoparticles in a copolymer to create a homogeneous composite with enhanced mechanical or electrical properties, an endeavor that requires strategies to prevent aggregation.[17] The second type of application aims to exert some degree of control over the nanoparticle location in inhomogeneous materials, such as the ordered phases of diblocks. By dispersing nanoparticles selectively in one domain, it is possible, for instance, to increase the dielectric contrast required for fabrication of photonic crystals.[18] Beyond photonic applications, nanocomposites hold considerable promise for the creation of new nanostructured materials, as demonstrated recently by the bicontinuous phase that arises when Janus-like nanoparticles are dispersed in a lamellae-forming diblock copolymer.[19] Finally, a third type of application would use ordered block copolymers as templates for hierarchical assembly of perfectly ordered arrays of nanoparticles. Such arrays would be of interest for a number of devices, including magnetic storage media or light-harvesting devices.

Nanoparticles generally consist of a solid metallic core that is usually surrounded by a "shell" of grafted, short polymer chains that facilitate dispersion in the polymeric melt. In the limit where the core radius R_c is much smaller than the shell R_s, the nanoparticle can be modeled as a star polymer.[20] On the other hand, in the limit of a large core with no shell, one recovers the case of a colloid. Alternatively, if the molecular weight of the grafted chains is high enough, the shell could be viewed as a brush, whose properties are well-known.[21] In practice, however, these limits are rarely attained, thereby making the theoretical description of the experimentally relevant nanoparticles particularly challenging. The detailed interaction between the nanoparticle and its surroundings involves the type and molecular weight of grafted chains, their areal density, and the type of metallic surface. Simulations at the atomistic level would probably be required to understand the details of such interactions. At the more coarse grain level considered in this work, the nanoparticle−copolymer interaction is taken into account through a phenomenological parameter.

Experiments indicate that nanoparticle/block copolymer composites exhibit a rich behavior. At low volume fractions, the nanoparticle's size and shell properties determine whether it is preferentially located at the interface or in the middle of a domain.[22,23] A high volume fractions, nanoparticles can induce a change in morphology.[24] In thin films, nanoparticles can influence the morphology or the orientation of domains.[25]

Theoretical studies of nanoparticle distribution in block copolymers have been limited. Thompson et al. combined a SCFT for the polymers with a hard-sphere density functional for the nanoparticles (SCFT-DFT method[26]). The SCFT-DFT approach has been used to predict the location of nanoparticles in a lamellar morphology and the effect of nanoparticles on the orientation of lamellae confined between two walls.[27] Other studies have focused on particle-induced changes in morphology, which can occur by changing the particle size or its interaction energy with the copolymer.[28] The case of bidisperse particles has also been considered.[29,30] The SCFT-DFT approach, however, suffers from several limitations. Given the computational demands of the SCFT itself, almost all SCFT-DFT calculations have been concerned with two-dimensional systems (one exception involves the bcc phase), implying that nanoparticles are actually disks, as opposed to spheres (or, if invariance in the third direction is assumed, the nanoparticles are infinitely long rods). Perhaps more importantly, the coupling between the nanoparticles and the polymer in published versions of the SCFT-DFT method is only approximate, and the consequences of such an approximation remain unclear.

More recently,[31] Sides et al. introduced a hybrid particle field method (HPF) to describe polymer nanocomposites. In contrast to the earlier SCFT-DFT approach, the HPF method retains the nanoparticle positions as explicit degrees of freedom, thereby ensuring a complete coupling between nanoparticle and copolymer degrees of freedom. The HPF approach offers the potential to take into account the effect of fluctuations and has been shown to be capable of describing the change in morphology that arises when nanoparticles are added to several block copolymer structures in the bulk. However, it is computationally intensive, and its application to date has been limited to 2D systems in the absence of fluctuations.

The coarse grain MC simulation method described in this work can be used in a straightforward manner to treat three-dimensional systems of nanoparticle/block copolymers. As the HPF method, the approach is hybrid in the sense that the interaction between polymer and that between polymer and particle are treated on a different footing: the former is taken into account via a functional of the local densities; the latter involves an explicit interaction potential. Our paper is organized as follows: Section II describes the coarse grain description of the polymer and nonpolymeric object, and it explains in general terms the MC simulation approach. Section III examines the accuracy of the method and the influence of the discretization scheme employed. In section IV we present a specific application involving nanoparticles and consider the case of a thin film on a patterned substrate for which experimental data are available.

II. Method

A. Model. The model considered in this work is designed to describe the properties of a block copolymer at mesoscopic length scales. It includes three main ingredients: the chain connectivity, the small compressibility of the melt, and the incompatibility between unlike monomers. Such a model has been described previously,[9] and we only recall its main characteristics here. Consider n AB block copolymer molecules in a volume V at temperature T. Each chain contour is discretized into N beads, with the position of the sth bead in the ith chain denoted by $\mathbf{r}_i(s)$. The interaction energy $\mathscr{H}$ includes the bonded (b) and nonbonded (nb) contributions:

$$\mathscr{H}[\{\mathbf{r}_i(s)\}] = \mathscr{H}_b[\{\mathbf{r}_i(s)\}] + \mathscr{H}_{nb}[\phi_A, \phi_B] \quad (1)$$

Note, however, that while bonded interactions are described through a pairwise interaction function between beads, nonbonded interactions are taken into account through a functional of the local densities $\phi_A(\mathbf{r})$ and $\phi_B(\mathbf{r})$. As explained below, those densities are computed from the bead positions.

In what follows, we consider Gaussian chains, for which the bonded interactions are represented by harmonic springs:

$$\frac{\mathscr{H}_b[\mathbf{r}(s)]}{k_B T} = \frac{3}{2}\sum_{s=1}^{N-1} \frac{[\mathbf{r}(s+1) - \mathbf{r}(s)]^2}{b^2} \quad (2)$$

where k_B is the Boltzmann constant, $b^2 = R_e^2/(N-1)$ is the mean-squared bond length, and R_e^2 is the mean-squared end-to-end distance for an isolated, noninteracting chain. For nonbonded interactions, we chose the simple form

$$\frac{\mathscr{H}_{nb}[\phi_A, \phi_B]}{k_B T} = \rho_0 \int_V d\mathbf{r}\, [\chi \phi_A \phi_B + \frac{\kappa}{2}(1 - \phi_A - \phi_B)^2] \quad (3)$$

where ρ_0 is the average bulk number density of beads (in the absence of nanoparticles). The incompatibility between unlike beads is described by a Flory−Huggins term, and its strength is controlled by χ. The Helfand quadratic approximation[32] of eq 3 restricts the fluctuations of the local densities away from the average value. The melt is thus given a finite compressibility, which is proportional to κ^{-1}. The resulting Hamiltonian can be expressed as

$$\frac{\mathscr{H}[\{\mathbf{r}_i(s)\}]}{k_B T} = \frac{3}{2}\sum_{i=1}^{n}\sum_{s=1}^{N-1} \frac{(N-1)[\mathbf{r}_i(s+1) - \mathbf{r}_i(s)]^2}{R_e^2} + \sqrt{\bar{N}} \int_V \frac{d\mathbf{r}}{R_e^3}\left[\chi N \phi_A \phi_B + \frac{\kappa N}{2}(1 - \phi_A - \phi_B)^2\right] \quad (4)$$

From eq 4 it is apparent that the model and our simulations rely on only a few coarse grain parameters. The first is R_e, which sets the length scale for our coarse grain representation. The strength of fluctuations is controlled by the interdigitation number $\sqrt{\bar{N}} = \rho_0 R_e^3/N$, which provides an estimate of the number of chains that a given chain interacts with ($\bar{N}$ is referred to as the invariant degree of polymerization since in a dense melt it is proportional to the molecular weight). The two other parameters are the products χN and κN, implying that the chain contour discretization N is not a physical parameter in itself.

B. Definition of Local Densities. The Hamiltonian given by eq 4 defines a coarse grain model for a polymer melt. That Hamiltonian can be taken as the starting point for SCFT.[1] However, in SCFT the degrees of freedom are the local densities or fields. By assuming that the chain conformation is always in equilibrium with the fields, the configurational degrees of freedom have been integrated out. In our MC simulations we follow a different path: the local densities are defined from the beads' positions, which remain the fundamental degrees of freedom.

1. General Considerations. The local densities that enter eq 3 are not given by the microscopic expression $\phi_A(\mathbf{r}) = \sum_{i\in A \text{ bead}} \delta(\mathbf{r} - \mathbf{r}_i)$. Rather, the local densities are obtained from the bead position by a smoothing procedure, for which several possibilities can be considered. One choice is to associate to each bead a cloud density, so that $\phi_A(\mathbf{r}) = \sum_{i\in A \text{ bead}} g(\mathbf{r} - \mathbf{r}_i)$, where the cloud function g is for instance a Gaussian (up to a cutoff). A second possibility is to use a "particle-to-mesh" (PM) technique, where a regular mesh (or grid) is introduced and local densities are defined on each node (or site).

Regardless of the choice of technique, be it based on a density cloud or a PM scheme, it is necessary to introduce a discretization parameter, denoted as ΔL. That parameter is given by the Gaussian width in the cloud-density method and by the grid spacing in PM-based schemes. Within our proposed approach, length scales much smaller than ΔL cannot be described accurately. The parameter ΔL therefore defines a microscopic cutoff whose value is determined by several considerations. On the one hand, it determines the range of interaction between neighboring beads. This implies that ΔL cannot be smaller that the mean distance between beads, in which case they would barely interact.[57] On the other hand, ΔL cannot be too large, lest the ability to resolve an inhomogeneous density distribution be lost; ΔL should not be much larger than the typical length over which the density exhibits significant variations (e.g., the width of an interface between an A-rich and B-rich domain). In view of those two constraints, ΔL should be set at the smallest value that maintains a reasonably large number of interacting beads (which is denoted as n_{int} in what follows). As expected, the actual value of ΔL to be used for a given problem depends on the smoothing procedure and on the specific example of interest.

The cloud-density technique requires that all pairs of beads that are close enough to interact be identified; it is therefore more computationally demanding than the PM technique. While it avoids some of the artifacts related to the introduction of a grid, the additional resolution that is gained is generally of little relevance. We note that ref 13 reports that cloud-density and PM-based schemes give essentially the same results. In the interest of brevity, our discussion is mainly focused on the PM scheme at various levels of interpolation. In a forthcoming publication, we will present a detailed analysis of the cloud-density approach.

2. Details of Implementation. We now describe our particular implementation of the PM procedure (pth order assignment "a la Hockney and Eastwood"[33]). Particle-to-mesh (PM) techniques have been discussed in the context of efficient computation of Ewald sums.[34] As illustrated in Figure 1, local densities are defined on the n_{site} sites of a regular grid. A bead at position $\mathbf{r}$ yields a contribution to the pth site given by $W(\mathbf{r} - \mathbf{r}(p))$, where $\mathbf{r}(p)$ is the site position and $W(\mathbf{r})$ is an assignment function. For simplicity and ease of implementation, the same assignment function is used independently in each direction, that is, $W(\mathbf{r}) = W(x)W(y)W(z)$. The normalized A density at site p is

$$\phi_A(p) = \frac{1}{\rho^{nor}(p)} \sum_{i\in A \text{ bead}} W(\mathbf{r}_i - \mathbf{r}(p)) \quad (5)$$

The normalization constant $\rho^{nor}(p)$ represents the total density that would be observed at site p in a perfectly homogeneous system. In the simplest case, it is given by $\rho^{nor} = nN/n_{site}$ (some exceptions will be discussed below).

While interpolation schemes of arbitrary order are possible, only the zeroth- and first-order schemes are considered here. The corresponding one-dimensional functions $W(x)$ are shown in Figure 1. In the zeroth-order scheme, referred to as PM_0, the

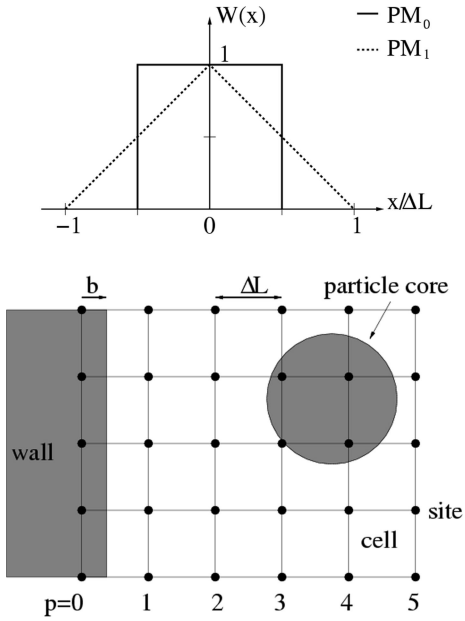

Figure 1. (top) Assignment functions for the PM_0 and PM_1 interpolation schemes. (bottom) Schematics of the grid used in the PM technique to compute the local densities. In the presence of a hard wall or a particle with hard core, the normalized densities $\rho^{nor}(p)$ become site dependent and are given by eq 15.

entire weight of a bead is assigned to the nearest grid site, irrespective of its position relative to the site. This implies that two beads interact only when they are assigned to the same site. The local density $\phi_A(p)$ is restricted to a discrete set of values, given by i/n_{int}, $i \gtrsim 0$. In this case, it is important that n_{int} be large enough so as to minimize the discretization of $\phi_A(p)$ (taking $n_{int} = 1$ for instance would lead to $\phi_A(p) = 0, 1, 2, ...$). From considerations given earlier, n_{int} actually determines a minimum value for the grid spacing, namely $\Delta L = (n_{int}/\rho_0)^{1/3}$. In contrast, the first-order scheme (referred to as PM_1) distributes a bead's contribution among its eight neighboring sites; two beads interact as soon as they are in neighboring cells, and $\phi_A(p)$ now varies in a continuous manner with the bead positions. A somewhat smaller ΔL can be employed with the first-order scheme.

C. Substrates and Nonpolymeric Objects. The model defined so far can only describe bulk polymeric systems. We now extend it to describe the effects of substrates and nonpolymeric objects. A solid surface is represented by a flat, hard wall that is impenetrable to polymer chains. Depending on the substrate properties and type of monomers, the interaction between the two might be attractive, repulsive, or neutral. To qualitatively reproduce those effects, the model substrate exerts on each bead a potential $U_S(\mathbf{r}, K)$, which depends on the bead's position $\mathbf{r}$ and its type K. The Hamiltonian then includes the additional term

$$\mathscr{H}_S = \sum_{\text{bead } i} U_S(\mathbf{r}_i, K_i) \tag{6}$$

Following earlier studies,[9] $U_S(\mathbf{r}, K)$ is defined as

$$\frac{U_S(\mathbf{r}, K)}{k_B T} = f_S(x, y, K)\frac{\Lambda_S}{2d_S}\exp\left[-\frac{z^2}{{d_S}^2}\right] \tag{7}$$

Here, the z-axis is normal to the substrate. In this direction, the potential decays over a distance d_S. Irrespective of the value of d_S, the strength of the interaction is controlled by $\Lambda_S N$. The function $f_S(x, y, K)$ has absolute value of unity, and its sign determines whether the surface exerts a local attraction or a repulsion toward a given type of bead. For a patterned substrate, $f_S(x, y, K)$ depends explicitly on x or y, while it is a constant for a homogeneous surface.

In experiments, the wetting properties of the substrate are often controlled with a coating of short polymer brushes. The explicit representation of those low molecular weight grafted chains could be achieved within the model presented here, but at the expense of a high resolution (high discretization of the contour of the chain, in particular). Since the spirit of the model is to describe properties on long length scales, this possibility is not considered in this work. The potential U_S is used instead as a simple means to represent the nature of the surface. As is often done in SCFT and molecular simulation studies, the free interface between air and polymer is modeled as a particular type of planar substrate. The possibility of nonplanar interfaces, deformed by terraces and holes, for instance, is not discussed in this work.

Non-polymeric objects dispersed in the polymer (or "particles", in what follows) can also be modeled as a potential acting explicitly on the polymer beads. Instead of being fixed, as is the case of the substrate, that potential is now mobile. This potential is denoted by $U_P(\mathbf{r}, K)$, where $\mathbf{r}$ is the vector joining the center of the object to the position of a bead. The potential can be chosen at will to represent the particle shape and the shell properties. For concreteness, we limit our discussion to the simple case of spherically symmetric particles; extensions to other situations (such as rods, platelets, or Janus-like nanoparticles) are straightforward. The potential $U_P(\mathbf{r}, K)$ is defined as follows:

$$\begin{aligned}\frac{U_P(\mathbf{r}, K)}{k_B T} &= \infty && \text{for } r < R_c \\ &= \frac{\Lambda_{PK}}{d_P}\exp\left[-\frac{(r-R_c)^2}{2{d_P}^2}\right] && \text{for } R_c < r < R \\ &= 0 && \text{otherwise}\end{aligned} \tag{8}$$

Here R_c denotes the core radius, and R is the total radius (core and shell). The solid core is thus impenetrable to polymer beads, and the affinity between beads of type K and the shell is controlled by $\Lambda_{PK}N$. The interaction energy between the nanoparticles and the beads is taken into account in the Hamiltonian with the term

$$\mathscr{H}_P = \sum_{\text{particle } p}\sum_{\text{bead } i} U_P(\mathbf{r}_i - \mathbf{r}_p, K_i) \tag{9}$$

D. Monte Carlo Simulations. Having defined our model, we determine its properties using a Monte Carlo (MC) approach that samples configurations according to their Boltzmann weight. In every MC move, trial positions are generated for an individual bead or a group of beads. The difference in energy ΔE between the original and the trial configuration determines the probability of accepting the move. When using the Metropolis criterion to accept or reject trial moves, this probability is given by $p_{acc} = \min[1, \exp(-\Delta E/k_B T)]$.

The energy change ΔE includes all contributions to the Hamiltonian: the change in bond length (bonded interactions) and local densities (nonbonded interactions) as well as the change of potential energy associated with the substrates and the particles. The simplest MC move consists of a random displacement of an individual bead. One of the advantages of the coarse grain MC approach proposed here, however, is that one can resort to fairly elaborate MC moves that have been developed over the past three decades to facilitate sampling in complex fluids and polymers. Some of the trial moves that are used in this work include reptation (with a single or multiple beads), translation of an entire chain, or switching the order of the blocks of a symmetric diblock copolymer molecule while

keeping the same chain conformation. In the case of particles, MC moves are usually restricted to translation and rotation for nonspherical particles; the energy change always includes a contribution from the potential energy. When the particles include a hard core, there is a change in the local densities as well (see below).

The simulation scheme is thus reduced to a regular MC algorithm with Metropolis sampling. The only unusual feature resides in the interaction potential between beads. In contrast to conventional pairwise interactions such as those arising from a Lennard-Jones potential energy function, the interaction between two beads is anisotropic and lacks translational invariance because it depends not only on the bead's relative positions but, within a *PM* scheme, also on their position with respect to a grid. We emphasize again that the main reason for using a "grid-mediated" potential is that it provides a reasonable description of properties on long length scales, and it allows for a fast evaluation of the energy. Updating the local densities is faster (and simpler, implementation-wise) than computing interactions between all pairs of beads.

The interaction between beads does not include a hard core; chains can therefore cross each other, and in the present form our model cannot be used to describe the dynamics at the level of a single chain. Note, however, that by restricting the trial moves in the MC algorithm to simple, physically realistic local moves (e.g., local random displacements), it is possible to recover physically realistic dynamics, if entanglement effects are weak. We also note that the soft potentials that arise from coarse graining are a typical feature of mesoscopic modeling approaches,[35] including dissipative particle dynamics[36–39] and models of highly coarse grained polymeric molecules.[40,41]

At this point it is instructive to emphasize the differences and similarities between the coarse grain MC method proposed here and SCMF simulations.[9,10] In SCMF simulations, the free energy is expressed using fields, in complete analogy to SCFT:

$$\frac{\mathscr{H}_{\mathrm{nb}}[\phi_{\mathrm{A}},\phi_{\mathrm{B}},w_{\mathrm{A}},w_{\mathrm{B}}]}{k_{\mathrm{B}}T}=\frac{\rho_0}{2}\int_V \mathrm{d}\mathbf{r}\,[\phi_{\mathrm{A}}w_{\mathrm{A}}+\phi_{\mathrm{B}}w_{\mathrm{B}}] \qquad (10)$$

where the fields are given by

$$w_{\mathrm{A}}=\chi\phi_{\mathrm{B}}-\kappa(1-\phi_{\mathrm{A}}-\phi_{\mathrm{B}})$$
$$w_{\mathrm{B}}=\chi\phi_{\mathrm{A}}-\kappa(1-\phi_{\mathrm{A}}-\phi_{\mathrm{B}}) \qquad (11)$$

A SCMF simulation consists of repeating the following two steps: (i) perform a short MC simulation of the chains in the fields w_{A} and w_{B}, with interaction given by eq 10, and (ii) from the bead positions, compute the new local densities and update the fields according to eq 11. A simulation is then run until a stationary state is attained. Even then, the fields are not static quantities but they fluctuate in "time" (that is, from one MC cycle to the next). For a given value of the fields, chains evolve independently from one another. The temporary decoupling between fields and instantaneous chain configurations implies that the energy change associated with a Monte Carlo move is only an approximation of the exact expression given by eq 3. As discussed in ref 10, the quality of such a "quasi-instantaneous field approximation" is controlled by a parameter ε that involves the discretization parameters ΔL and N. While one can choose ε so as to reach a desired level of accuracy, the coarse grain simulations described here do not involve that approximation.

Both MC simulations and SCMF simulations should recover the SCFT solution when $\sqrt{\bar{\mathcal{N}}} \to \infty$, with local densities becoming static quantities. Note, however, that working in this limit is not computationally advantageous since the system must then include a large number of beads.

E. Choice of Parameters. The parameters of the model include the four physical invariants (R_{e}, χN, κN, $\bar{\mathcal{N}}$) and two discretization parameters (N and ΔL). From knowledge of the experimental value of χ and taking N to be the degree of polymerization (number of monomers), one obtains the product χN. The parameter κ is related to the isothermal compressibility through $1/\kappa = -\rho_0 k_{\mathrm{B}}T/V(\partial V/\partial P)|_T$, where P is the pressure. As shown in previous studies, the value $\kappa N = 50$ is sufficiently large to prevent fluctuations of the total density on length scales larger than a fraction of R_{e}. The limit of an incompressible melt can not be addressed efficiently since the MC moves used in this work (the global ones, in particular) induce a local density fluctuation, leading to a low acceptance probability. The end-to-end distance R_{e}[58] is determined by comparing a theoretical and experimental characteristic length scale, such as the periodicity of a block copolymer morphology (note that R_{e} could also be computed from the statistical segment length found in the literature, but the uncertainty would probably be larger). Finally, the parameter $\bar{\mathcal{N}}$ can be computed from the melt density and the molecular weight used for a specific experiment.

As discussed earlier, the two discretization parameters N and ΔL are not independent: for a given N, a given bead should interact with a minimum number of beads (n_{int}), which translates into a minimum value for ΔL. The choice of N is dictated by the properties of interest and the specific details of the system under consideration. As shown below, an accurate description of the density profile of a polymer near a flat wall requires a high discretization ($N > 10^3$). With such a large number of degrees of freedom per chain, only small systems can be considered (a few R_{e}^3). The coarse grain model is primarily designed to study properties on long length scales; large systems are therefore required (many R_{e}^3), thereby calling for a low N. There is, however, a limit to how low the chain discretization N can be, lest the Gaussian statistics of the chain be lost.

F. Stress Tensor. Within the mean field approximation the internal stress tensor is given by[42]

$$\frac{\sigma_{\alpha\beta}}{k_{\mathrm{B}}T}=-\frac{nN}{V}I_{\alpha\beta}+\frac{3}{V}\sum_{i=1}^{n}\sum_{s=1}^{N-1}\left\langle\frac{N-1}{R_{\mathrm{e}}^{\,2}}\,\mathrm{b}_{i,\alpha}(s)\,\mathrm{b}_{i,\beta}(s)\right\rangle \qquad (12)$$

where I is the identity tensor, $\alpha, \beta \in \{x, y, z\}$, $\mathbf{b}_i(s) = \mathbf{b}_i(s+1) - \mathbf{b}_i(s)$ is the bond vector joining two adjacent beads, and $\langle\,\rangle$ denotes a thermal average. The stress tensor is useful to approximately determine the equilibrium periodicity of a given morphology. In the case of bulk lamellae, for instance, the stress is computed as a function of the lamellar spacing. The equilibrium lamellar spacing is reached when σ is isotropic. Alternatively, a variable cell shape method can be used. Such a method, originally introduced by Parinello, Ray, and Ramhan to describe crystalline structures in solids,[43,44] has recently been implemented in the context of SCFT.[45,46] As described in ref 47, its implementation in our coarse grain MC simulations is straightforward.

III. Analysis of Discretization Effects

The model is characterized by the physical invariants (R_{e}, χN, κN, $\bar{\mathcal{N}}$) and the discretization parameters (N, ΔL, and the smoothing procedure). In the limit of high discretization ($N \to \infty$, $\Delta L \to 0$), one can expect the system properties to reach a well-defined limit, independent of the details of discretization. In this section we show that, in some situations, this limit is only reached for conditions that would place constraints on the type of phenomena that can be investigated. It is therefore necessary to gauge the effects of finite discretization levels that are of practical significance. Understanding such effects is particularly important in situations such as those considered in our work, where the particles have a size comparable to the grid spacing ΔL and the bond length b. As discussed in what follows, our conclusions are valid for the set of physical

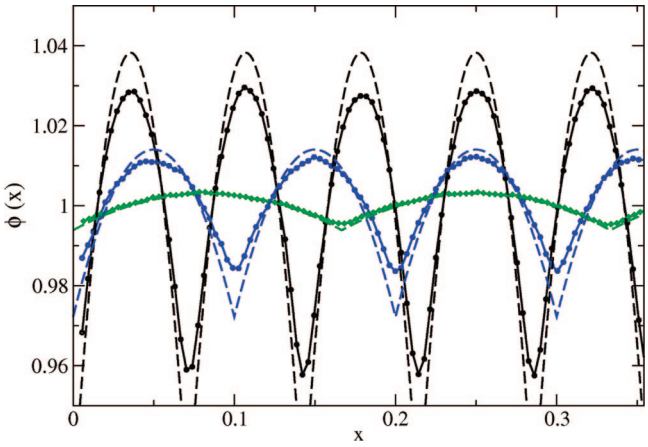

Figure 2. Average density profile for a bulk homopolymer. The grid spacing ΔL is 0.07, 0.1, and 0.17 R_e (black, blue, and green curve, respectively). The dashed lines are the predictions of an approximate treatment (see text). The oscillations are an artifact of the PM_1 scheme used.

invariants considered in this work, which are rather typical of a block copolymer melt. Applications to a different type of system would require that a study of discretization effects analogous to that presented here be performed on such a system. In the interest of conciseness, we discuss discretization effects in four representative limits, namely a homopolymer in the bulk, a confined homopolymer, the interface between domains in lamellae-forming systems, and a single particle dispersed in a homopolymer. When appropriate, the computation of local densities is also explained in detail.

A. Bulk Homopolymer. The bulk homopolymer is the simplest nontrivial situation that we consider. Here the contour discretization N is set to 32. We focus on the average density profile, computed along the x-axis of the grid. When using a PM_0 scheme, the density profile is constant and equal to unity, as it should be. This is not the case, however, when using the PM_1 scheme, as shown in Figure 2. The density exhibits periodic oscillations, with maxima that correspond to the middle of each cell.[59] The amplitude of the oscillations increases when decreasing ΔL, reaching 5% for $\Delta L = 0.07\ R_e$.

To develop an understanding of those effects, consider the simple case of a one-dimensional system containing only monomers, that is, beads without bonds between them. The Hamiltonian is then given by

$$\frac{\mathscr{H}}{k_B T} = \frac{\kappa \rho^{nor}}{2} \sum_{\text{site } p} [\phi(p) - 1]^2 = \frac{\kappa}{2\rho^{nor}} \sum_{\text{site } p} [\rho(p) - \rho^{nor}]^2 \quad (13)$$

where $\rho(p) = \rho^{nor}\phi(p)$ is the un-normalized density at site p. We consider a polymer bead and denote by x_l (x_r) the coordinate of the grid site to the left of the bead (right). The bead's position x can be expressed as $x = (x_l + x_r)/2 + \Delta L \delta x$, where $|\delta x| \leq 1/2$. When using the PM_1 scheme, the density on the site on the left is given by $\rho_l = \rho_l' + 1/2 - \delta x$, where $1/2 - \delta x$ is the contribution of the bead under consideration, and ρ_l' represents the contribution of all other beads. The energy associated with the sites on the left and the right is thus

$$\frac{E}{k_B T} = \frac{\kappa}{2\rho^{nor}}\left[(\rho_l' + 1/2 - \delta x - \rho^{nor})^2 + (\rho_r' + 1/2 + \delta x - \rho^{nor})^2\right] = \frac{\kappa}{2\rho^{nor}}\left[(\rho_l' + 1/2 - \rho^{nor})^2 + (\rho_r' + 1/2 - \rho^{nor})^2 + 2\delta x(\rho_r' - \rho_l') + 2\delta x^2\right] \quad (14)$$

For simplicity, we proceed with a "mean field" approximation that replaces ρ_r' and ρ_l' by their average value $\langle \rho_r' \rangle = \langle \rho_l' \rangle$; the equality holds because the system is homogeneous. The probability to find a particle at position δx is thus given by $\mathscr{P}(\delta x) = C \exp[-\kappa \delta x^2/\rho^{nor}]$ where C is a normalization constant such that $\int_{|\delta x| \leq 1/2} du\ \mathscr{P}(u) = 1$. One can also estimate the average energy δE that a bead gains when optimizing its position with respect to the grid. Taking $\langle \delta x^2 \rangle = 1/12$, which only holds for a strictly uniform distribution of beads, one finds $\delta E \simeq \kappa k_B T/(12\rho^{nor})$. If all the beads register with the grid, the total energy gain is of order $\kappa N n_{site} k_B T/(12N)$, which is not negligible and increases with system size.

It is straightforward to extend the above calculation to three dimensions, although we no longer have a simple closed-form expression. The corresponding density profiles, which we have computed numerically, are shown in Figure 2. The agreement between our numerical solution and the results of simulations is good for the largest grid spacing $\Delta L = 0.17\ R_e$, but it deteriorates for smaller ΔL, as the "mean field" approximation becomes less justified. These results demonstrate that the oscillations observed in the density profiles of Figure 2 are merely a well-defined numerical artifact introduced by the use of the grid. As such, one can think of several numerical strategies to mitigate those spurious grid-induced oscillations. When the grid spacing is large and the approximate treatment sufficiently accurate, a periodic potential can be added to the Hamiltonian to compensate for the grid's influence. A different possibility is to get rid of the grid altogether. The normalized density is now defined not only at the grid sites but at every point in space, by an expression similar to that given in eq 5. As noted earlier, the simulation becomes more demanding because it is necessary to determine all pairs of beads that are close enough to interact. A third approach is to shift the grid in a random manner, thereby preventing the system from settling into the local energy wells introduced by a fixed grid. This approach has the advantage of being computationally efficient. However, the random motion of the grid does not represent a traditional MC move and is not subject to a Metropolis criterion. This third approach leads to an average density profile in bulk homopolymer that is perfectly flat, as it should. In other situations, such a lamellar diblocks, this procedure gives results very similar to those obtained with the "gridless" method (an analysis of that method will be reported in a future publication).

B. Confined Homopolymer. In the presence of a hard wall, the use of a shifting grid entails a few details that must be considered for the computation of local densities. Indeed, since the cells touching the wall are truncated, the normalized density $\rho^{nor}(p)$ at site p is not equal to nN/n_{site} but given by

$$\rho^{nor}(p) = \rho_0 \int_{V'} d\mathbf{r}\ W(\mathbf{r} - \mathbf{r}(p)) \quad (15)$$

where V' is the space accessible to the polymer beads. When using the PM_0 scheme, $\rho^{nor}(p)$ is simply proportional to the volume of the cell associated with site p. Simple formulas are also available for the PM_1 case. For simplicity and concreteness, we consider the case described in Figure 1, where the grid is shifted by a distance $0 \leq b < \Delta L$ from the wall. The normalized densities are then given by

$$\begin{aligned} \rho^{nor}(0) &= \rho_0 \Delta L^3 \frac{1}{2}\left(1 - \frac{b}{\Delta L}\right)^2 \\ \rho^{nor}(1) &= \rho_0 \Delta L^3 \frac{1}{2}\left[2 - \left(\frac{b}{\Delta L}\right)^2\right] \\ \rho^{nor}(p \geq 2) &= \rho_0 \Delta L^3 \end{aligned} \quad (16)$$

We now consider a homopolymer confined in a slit of width $L_z = 1\ R_e$. In the vicinity of the surface, the polymer melt exhibits a depletion layer. Its width is related to the Edwards correlation length ξ that depends only on the compressibility: $\xi/R_e = 1/(12\kappa N)^{1/2}$. We fix ΔL so that $n_{int} \simeq 15$ for PM_0 and

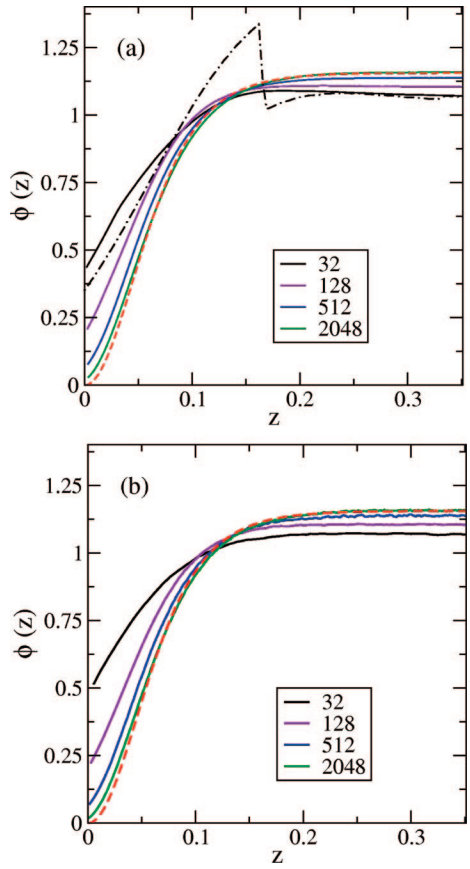

Figure 3. Average density profiles for a homopolymer confined in a slit of width $L_z = 1\ R_e$, computed with various contour discretizations N. The interpolation scheme is either PM_0 (a) or PM_1 (b). The dashed line is a fit according to eq 17 for the curve with $N = 2048$. The dotted-dashed line in (a) represents the profile obtained with $N = 32$ and a fixed grid.

$n_{int} \simeq 30$ for PM_1.[60] Figure 3 shows the averaged density profiles computed with the PM_0 and PM_1 schemes, for N in the range from 32 to 2048 (ΔL ranges from 0.15 to 0.04 R_e). Figure 3a also shows the curve obtained with $N = 32$ and a fixed grid. This curve exhibits a large discontinuity at the boundary cell $x = \Delta L$. This artifact, visible whenever the grid is fixed, is the main reason to shift the grid in the PM_0 scheme. Using a shifting grid yields a curve which is smooth but that can exhibit a maximum depending on the level of discretization. Only when a larger discretization N is employed does the maximum disappear. Density profiles for the PM_1 scheme (and a shifting grid) do not show any maxima, confirming that this is an artifact of the PM_0 implementation. Whatever PM scheme is used, however, the resulting density profiles are strongly dependent on N, particularly at wall contact. This can be understood by considering the average bond length: for $N = 32$, b ($\simeq 0.18\ R_e$) is actually larger than the depletion layer, while for $N = 2048$, b ($\simeq 0.022\ R_e$) is much smaller. In the former case, the contour discretization is too large to faithfully describe the Gaussian statistics of the chains in the immediate vicinity of the wall. Figure 3 also shows the density profile obtained by the ground-state approximation in the limit of large $\sqrt{\bar{N}}$, namely

$$\phi(z) = a^2\left[\tanh\left(\frac{az}{2\xi}\right) + \tanh\left(\frac{a(L_z - z)}{2\xi}\right) - \tanh\left(\frac{aL_z}{2\xi}\right)\right]^2 \quad (17)$$

where a is a normalization constant such that $\int_0^{L_z} dz\ \phi(z) = L_z$.[4] Given that $\sqrt{\bar{N}} = 128$, eq 17 can be expected to be reasonably accurate. Indeed, it provides a good fit for the most accurate profiles computed in this work ($N = 2048$) and yields in both cases an effective screening length $\xi/R_e = 0.037$ that is in good agreement with the theoretically expected value of $\xi/R_e = 1/(12\kappa N)^{1/2} \simeq 0.041$. Higher levels of discretization would lead to even better agreement, but they are of little practical interest.

Table 1. Parameters Used in Discretization Schemes (Left) and Corresponding Lamellar Spacings Obtained in the Three Systems (Right)

discretization parameters				lamellar spacing L_0		
scheme	N	ΔL (R_e)	PM	diblock	blend 1	blend 2
S1	32	0.15	0	1.80	2.05	2.45
S2	32	0.1	0	1.80	2.03	2.42
S3	32	0.1	1	1.79	2.05	2.47
S4	128	0.1	1	1.80	2.07	2.50

Table 2. Description of Polymer Systems Considered in This Study[a]

species	f_A	MW	diblock	blend 1	blend 2
copolymer	15/32	1	100	80	60
homopolymer A	1	7/16	0	10	20
homopolymer B	0	7/16	0	10	20

[a] For each species, the fraction of A beads f_A, the molecular weight relative to the diblock (MW), and the volume fraction in the system are given.

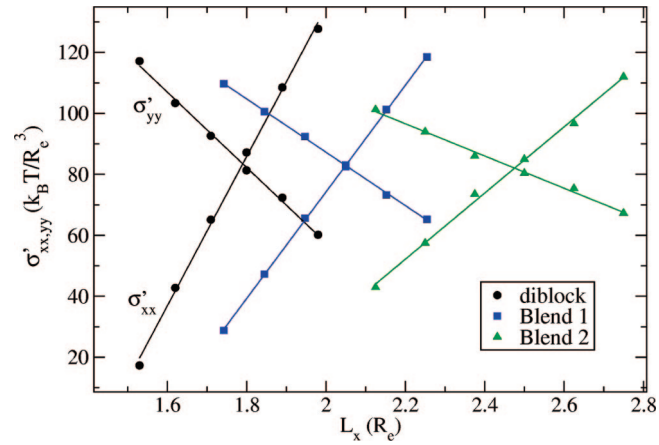

Figure 4. Stress tensor as a function of an imposed periodicity L_x for three lamellae-forming systems, confined between two neutral surfaces. The thickness of the film is $L_z = 1.5\ R_e$. The lamellae are oriented normal to the surfaces and perpendicular to the x-axis. The tensor $\sigma' = \sigma - \mathrm{Tr}(\sigma)/3I$ is the anisotropic part of the stress tensor defined in eq 12. The nondiagonal components of the stress tensor vanish. The lines are linear fits to the numerical results of MC simulations. The equilibrium lamellar spacing is reached when $\sigma'_{xx} = \sigma'_{yy}$, which gives $L_0 = 1.79$, 2.05, and 2.47 R_e for the diblock, blend 1, and blend 2, respectively.

C. Interface in Lamellae-Forming Systems. We now focus on the density profile at the interface between an A-rich and a B-rich domain. In the limit of large χN, the intrinsic width w of the interface is given by $w/R_e = 1/(6\chi N)^{1/2}$. To gauge the effect of discretization, we have computed density profiles using four distinct discretization schemes. The details of each scheme are described in Table 1. Three lamellae-forming systems are considered: a pure AB diblock and two ternary blends, including a mixture of the diblock with equal amounts of homopolymer A and B. Table 2 gives the parameters for each molecule and the composition of each system. The polymer is confined between two neutral hard walls, representing a thin film of thickness $L_z = 1.5\ R_e$. The x-axis is chosen perpendicular to the lamellae.

The lamellar spacing is determined by computing the stress tensor as a function of the imposed periodicity. Figure 4 gives an example of the stress−periodicity curves that arise for different systems; they are generally linear in the range

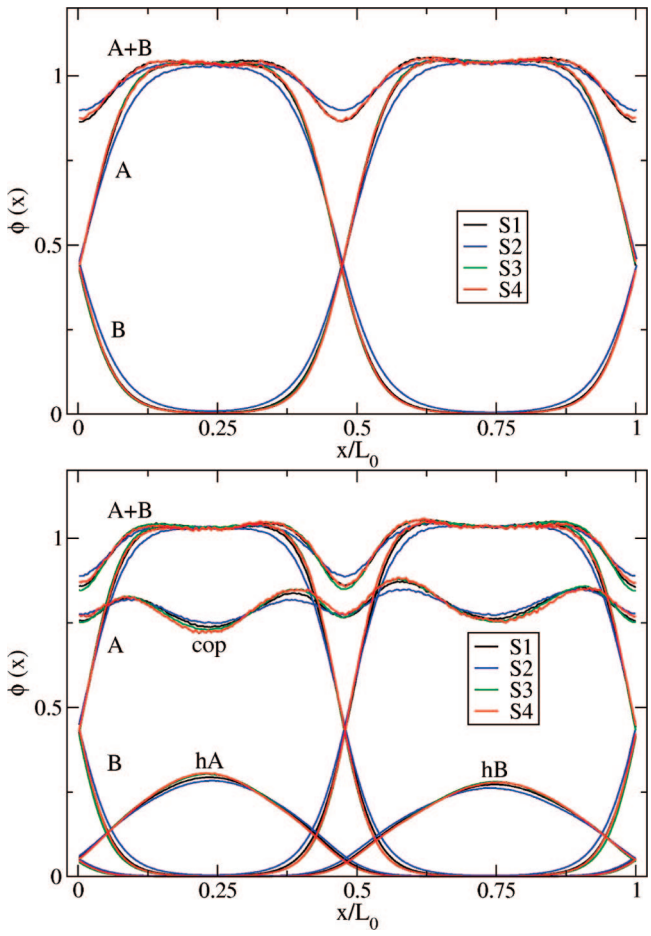

Figure 5. Influence of the discretization scheme on the average density profiles for a thin film of the pure diblock copolymer (top) and blend 1 (bottom). Parameters are given in the text. The four discretization schemes (S1, S2, S3, S4) are defined in Table 1. Profiles for the A density (A), B density (B), and total density (A + B) are plotted. For the blend, profiles for the copolymer density (cop), homopolymer A (hA), and homopolymer B (hB) are also included.

considered in this work. The slope of the stress vs strain curves (not shown) gives the Young's (or tensile) modulus. As expected, it is smaller for the blends since the homopolymers help accommodate the compression or stretching of the lamellae. Note that since the system is confined, the stress tensor is anisotropic; the equilibrium condition that applies here is $\sigma_{xx} = \sigma_{yy}$.[61] The lamellar spacings are given in Table 1, and they differ from each other by, at most, a few percent.

The average density profiles along the x-axis provide a more stringent test of the effects of discretization.[62] They are plotted in Figure 5a for the pure diblock. The A and B domains have different width because the diblock is slightly asymmetric. The discretization schemes S1, S3, and S4 yield curves that are very similar to each other. This is particularly noticeable for schemes S1 and S4: although the *PM* levels are different and the bond lengths b differ by a factor of 2 ($b \simeq 0.18\,R_e$ and $0.09\,R_e$, respectively), the density profiles are almost identical. This observation suggests that a fine discretization, with a bond length much smaller than the interface width, is not necessary to obtain profiles that are independent of N. This observation is in contrast with the case of a depletion layer near a hard wall, where a correct limiting behavior is attained only for $N \geq 10^3$. The profiles obtained with scheme S2 clearly deviate from the others, with an interface that is significantly broader. The PM_0 scheme was employed in scheme S2, and the average number of beads per cell was low, namely $n_{cell} \simeq 4$, implying that the local densities can only adopt a restricted set of values (specifically i/n_{cell} with $i \geq 0$, approximately 0, 0.25, 0.5, 0.75, ...). Accordingly, one can expect strong discretization effects and results of low accuracy in that case. The conclusions reached with the pure diblock also hold for blend 1, as shown in Figure 5b. In addition to the densities of A and B beads, the profiles for the volume fraction of each species of the blend are plotted. Again the curves computed with the scheme S1, S3, and S4 are very similar to each other.

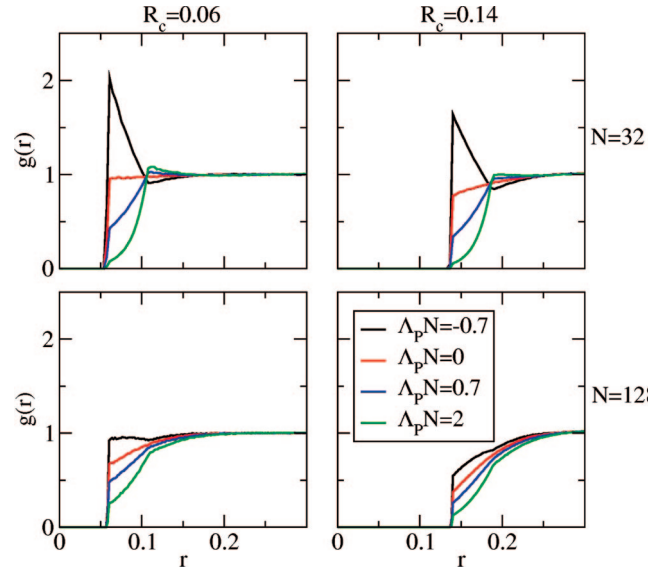

Figure 6. Pair correlation function between the particle center and the polymer beads, computed in the bulk homopolymer, for various surface potentials $\Lambda_P N$. The core radius is $R_c = 0.06\,R_e$ (left) or $R_c = 0.14\,R_e$ (right); the contour discretization parameter is $N = 32$ (top) or $N = 128$ (bottom).

D. Nanoparticle in Homopolymer. The hard core of a particle modifies the computation of the normalized local densities in a manner that is analogous to that discussed in the context of a hard wall. Indeed, in the absence of a correction, the local densities in the vicinity of the particle would appear artificially low, and the compressibility constraint would then induce a spurious attraction of the polymer toward the hard core. The correct normalized densities $\rho^{nor}(p)$ are given by eq 15. Each particle induces in the neighboring sites a correction that depends on their relative positions. Since the correction also depends on the core shape, it cannot, in general, be computed analytically. In practice, the corrections are evaluated and tabulated at the beginning of the simulation. Also note that the displacement of a particle induces a change in the local densities in the neighboring sites, even though the polymer beads are not actually moved in the process; the corresponding change in energy must be included in the acceptance criterion of the MC simulation.

We consider a nanoparticle described by the potential of eq 8. The particle has a core radius $R_c = 0.06\,R_e$ or $R_c = 0.14\,R_e$, with $R - R_c = 0.05\,R_e$ in both cases. The decay length d_P is set to $0.02\,R_e$, so that the interaction potential becomes negligible for $r > R$. To gauge the discretization effects, we have computed the pair correlation function between the nanoparticle center and the polymer beads. Figure 6 shows the results obtained with PM_1, contour discretizations $N = 32$ and $N = 128$, and various strengths of the surface potential $\Lambda_P N$. As expected, repulsive or attractive particles have their shell depleted or enriched in polymer beads, respectively. A discontinuity in slope is observed at $r = R$, where the particle potential vanishes. It is also apparent that, for a given N, the distribution of beads is governed mainly by the surface potential, since the profile depends only weakly

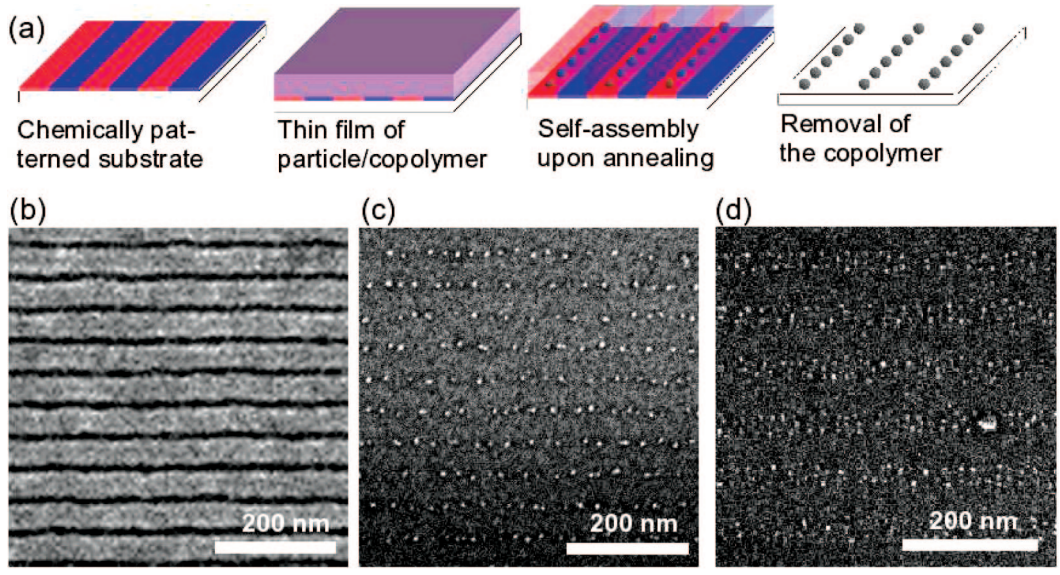

Figure 7. (a) Schematics of the experimental process. (b, c) Top-down SEM images of the system before and after removal of the polymer. In the latter, the particle cores appear as small white dots. The copolymer used is the diblock and $L_S/L_0 = 1.07$. (d) Same as (c) with blend 2 and $L_S/L_0 = 1.06$.

on the particle radius. On the other hand, the curves depend heavily on N, particularly for the attractive potential.

The case of a neutral particle is particularly interesting because the bead distribution is controlled by a balance between the entropic effects and the compressibility constraint. For $N = 32$, the depletion shell is hardly visible. This is not surprising, considering that the bond length $b \simeq 0.18\ R_e$ is almost as large as the hard-core diameter. While the volume forbidden to the polymer beads still restricts the conformation of the chains in the neighborhood of the particle, the bond length is not small enough to avoid discretization effects in the vicinity of the surface. For $N = 128$, the depletion shell becomes significant. As in the case of a flat surface, the depletion would further develop with increasing N, reaching its asymptotic limit only for $N > 10^3$. In general, a low contour discretization leads to underestimation of the entropic loss of polymers in the vicinity of the particle, thereby making it appear more attractive. One way of estimating the effective interaction at different N would be to compute the insertion free energy of the particle in the polymer. When considering nanoparticles, it is therefore important to retain the contour discretization N as an explicit parameter of a model because results obtained with different N can differ at even a qualitative level. For instance, if several particles are dispersed in the homopolymer, the depletion shell that arises at high N leads to particle aggregation, while this does not occur at lower N.

IV. Nanoparticle/Block Copolymer Thin Films on a Patterned Substrate

Having established the validity of our proposed approach, we apply our MC approach to investigate recent experiments involving mixtures of nanoparticles and a lamellae-forming block copolymer laid over a patterned substrate. The system considered here is fundamentally different from that of previous studies of copolymer composites in several respects. First, most theoretical studies have focused on the bulk properties of nanoparticle/block copolymer mixtures and on large nanoparticles and/or high volume fractions. Only the SCF-DFT method was used to study the influence of confinement between solid surfaces;[27] in that work, the surfaces were identical and homogeneous. In our work, only the top surface is homogeneous; the bottom surface is now patterned. Second, in addition to a pure diblock, we consider the case of ternary blends, made of AB copolymer, homopolymer A, and homopolymer B. Third, the nanoparticles are small ($R = 0.1\ R_e$), and their volume fraction is low (around 1%). These last three departures from previous work are important for a number of reasons. By considering a patterned substrate, it becomes possible to stretch or compress the block copolymer domains in a controlled manner, thereby providing a much more stringent test of the theory. By considering blends, it becomes possible to examine the interplay between local composition and nanoparticle position. And by considering truly nanoscopic particles (much smaller than the polymer), we can induce a weak disruption of the chain and have the particles act as probes of the polymer chains. Packing effects are not expected to be important for the conditions considered here. Perhaps more importantly, newly acquired experimental data are available for the system considered in this work.

A. Experimental System and Parameters. The specific experimental results we address below are described in detail in ref 48. Here we only recall the main points of an experimental procedure that is summarized in Figure 7a. A mixture of lamellae-forming copolymer and particles is spin-coated over a patterned substrate. The pattern consists of two kinds of stripes, each interacting preferentially with one of the blocks. If the pattern period (L_S) is close to the equilibrium lamellar spacing of the copolymer (L_0), the copolymer self-assembles into defect-free lamellae in registration with the underlying stripes.[53] The particles considered in this work have a shell that exhibits a strong preference for one block and therefore migrate into their preferred domain. The copolymer is subsequently removed by an oxygen plasma treatment, leaving behind an array of particles on the substrate. Figures 7b,c are top-down images of the system, obtained by scanning electron microscopy (SEM), before and after removal of the polymeric material. It has been verified experimentally that the particle distribution is not disturbed by the removal process to any significant extent.

The copolymer used in the experiments is a PS-*b*-PMMA diblock. Three distinct melts were employed, which we model with the parameters listed in Table 2 to match experimental conditions (as before, $\sqrt{\mathcal{N}} = 128$, $\kappa N = 50$, and $\chi N = 37$, and A and B stand for PS and PMMA, respectively). The experimental lamellar spacings are 49, 54, and 71 nm for the diblock,

blend 1, and blend 2, respectively. By direct comparison with the lamellar spacings found in simulations with the S3 discretization (see Table 1), one can deduce the simulated length scale that corresponds to each case, namely, $R_e \simeq 27.4$, 26.3, and 28.4 nm, respectively. Those length scales are reasonably close to each other, considering the uncertainties associated with both experimental and theoretical estimates.

Since the experimental film thickness is in the range $L_z = 40-45$ nm, we fix $L_z = 1.5\,R_e$ in our simulations. The substrate is patterned with parallel stripes of width $L_S/2$, designed to attract PS and PMMA blocks. Following previous studies,[9] we take $\Lambda_S N = 3$ and $d_S = 0.15\,R_e$. The function $f_S(x, y, A) = -f_S(x, y, B)$ adopts the value 1 or -1 depending on the stripe. The top free surface is represented by a hard neutral wall. Boundary conditions are periodic in the x and y directions.

The particles used in the experiment were made of a solid CdSe core, to which tetradecylphosphonic acid (TDPA) of low molecular weight was attached. TDPA chains exert a strong repulsion toward the PMMA block and a weak repulsion, if any, toward the PS block. These interactions drive the particles into the PS domains. In what follows, we take $R_c = 0.1\,R_e(\simeq 2.7$ nm) and $R = 0.15\,R_e(\simeq 4$ nm), consistent with experimental values. As previously, $d_P = 0.02\,R_e$. The value of $\Lambda_{PK}N$ is chosen below.

We chose the first order interpolation scheme PM_1, with a grid spacing $\Delta L = 0.1\,R_e$ (scheme S3 in Table 2). While it is more computationally demanding than the PM_0 scheme, it provides an enhanced accuracy that is likely to be important, particularly considering that the particle radius is comparable to the grid spacing ΔL. The simulation box includes two lamellae or more, and its width is at least $L_y = 3R_e$. Given the low volume fraction of particles (1%), the computation of average particle density profiles requires long time averaging over a single simulation or an average over distinct realizations, which is more amenable to parallel computations. The results shown below correspond to an average over 5−20 realizations, depending on the system.

B. Results. Before addressing the multicomponent blends studied in experiments, we begin by examining a few simpler cases that offer useful insights into the description and methods adopted in our work.

The first case involves a single particle in a pure homopolymer, confined between two hard, neutral flat walls. The slit width is $L_z = 1\,R_e$. The particle−polymer interaction is either attractive, neutral, or repulsive. Figures 8 and 9 show the distributions function for the center of the particle $\rho_{PC}(z)$; specifically, $\rho_{PC}(z)$ is proportional to the probability of finding the particle center at position z. On the one hand, as expected, the attractive particle avoids the vicinity of the wall, so as to preserve a layer of polymer in its shell. On the other hand, the repulsive particle sticks irreversibly to the walls, so as to minimize the unfavorable interaction between the polymer and the particle surface. The distribution of neutral particles is similar to that of the attractive particles. In particular, they both avoid the immediate vicinity of the walls. This effect is robust and insensitive to changes of the compressibility (up to $\kappa N = 500$) or to the use of a fixed or shifting grid.

We now examine the behavior of a single particle placed in the lamellar phase of the diblock. As was observed in simulations,[49,50] SCF-DFT,[51] and strong segregation theory calculations,[52] a neutral particle ($\Lambda_{PA}N = \Lambda_{PB}N = 0$) exhibits a preference for the interface, where it screens interactions between A and B polymer beads. For a particle repulsive to A and B blocks ($\Lambda_{PA}N = \Lambda_{PB}N = 2$), the localization at the interface is even stronger, and no particles are found in the middle of the domains. If the particle is repulsive to the B block and it is neutral with respect to the A block ($\Lambda_{PA}N = 0$, $\Lambda_{PB}N = 2$), it is driven to its preferred (A) domain, with a maximum probability of being located in the middle of the domain. Larger $\Lambda_{PB}N$ values do not seem to lead to significant changes in the particle distribution because the particle barely interacts with the B block. This last case is relevant to the nanoparticle experiments described above, to which we now turn our attention.

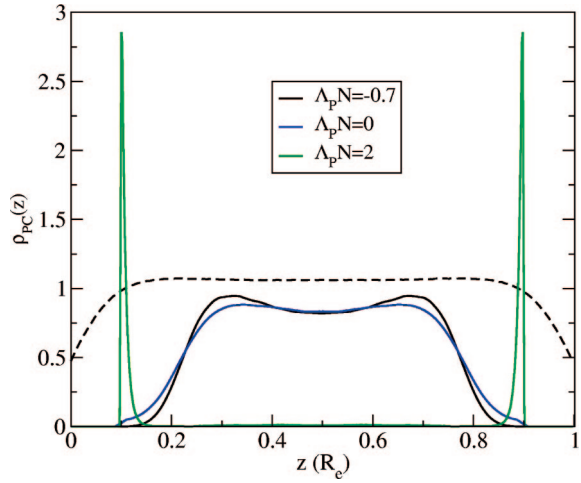

Figure 8. Distribution of particle placed in a homopolymer confined between two neutral flat walls. $\rho_{PC}(z)$ is proportional to the probability of finding the particle center at position z. The width of the slit is $L_z = 1\,R_e$. The particle−polymer interaction is attractive, neutral, or repulsive with $\Lambda_P N = -0.7$, 0, and 2, respectively. The dashed line is the polymer density profile.

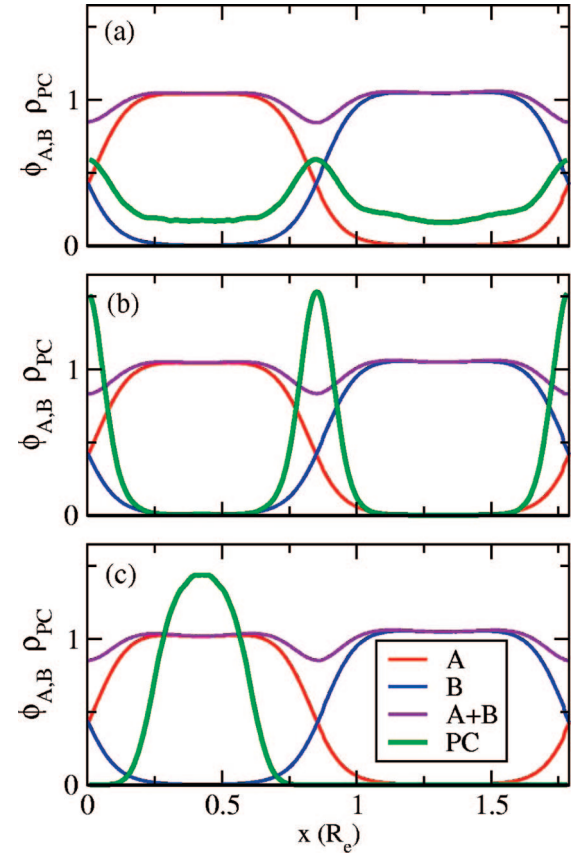

Figure 9. Distribution of particle center (PC) in the diblock for various interactions between particle and beads: (a) $\Lambda_{PA}N = \Lambda_{PB}N = 0$; (b) $\Lambda_{PA}N = \Lambda_{PB}N = 2$; (c) $\Lambda_{PA}N = 0$, $\Lambda_{PB}N = 2$. Also shown are the density profiles for A and B beads and the total polymer density (A + B).

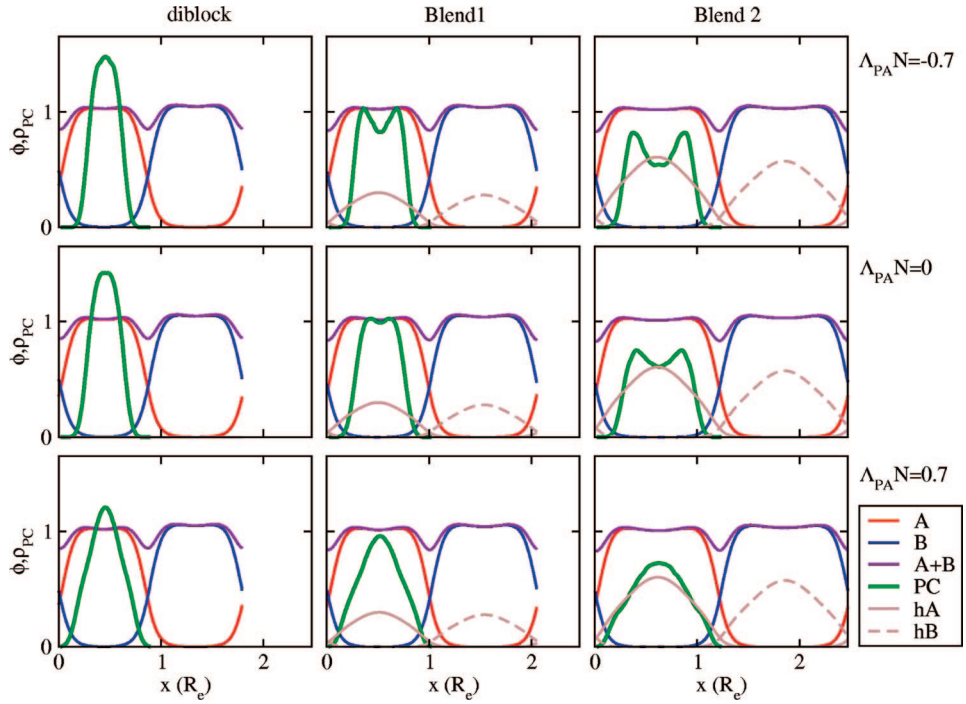

Figure 10. Distribution of particle center (PC) and density profiles in a thin film of diblock, blend 1, and blend 2, on a stripe-patterned substrate. The strong repulsion for the B block ($\Lambda_{PB}N = 2$) drives the particles in the A domain. The interaction with the A block is slightly attractive, neutral or slightly repulsive (from top to bottom). Also shown are the density profiles for A and B beads, for total polymer density (A + B) and for homopolymers (hA and hB).

Figure 10 shows the distribution of particles in a thin film for three mixtures on a patterned surface. The pattern period is commensurate with the bulk lamellar spacing ($L_S = L_0$) in all cases. The particles are strongly repulsive to the B block ($\Lambda_{PB}N = 2$), but the interaction with the A block is either slightly attractive, neutral, or slightly repulsive ($\Lambda_{PA}N = -0.7$, 0, and 0.7, respectively). All cases lead to similar results for the pure diblock; however, clear differences arise when homopolymer is added. The distribution profile for attractive particles shows two distinct peaks while, for the repulsive case, it remains single-peaked. Repulsive particles concentrate in the middle of the domain where the polymer density is lower, and the energetic penalty is minimized. In contrast, attractive particles are preferentially found at a small distance from the domain interface, in a region of high polymer density. The addition of homopolymer does not change significantly the particle distribution in the z direction (across the thickness of the film). In the case of slightly repulsive particles, a small fraction of them stick to the wall. Otherwise, particles are found throughout the film and exhibit a slight preference for the vicinity of the patterned substrate compared to the free surface. Note that in the experimental images of Figure 7b no particle is visible on the top free surface of the film, which is consistent with the results of our simulations.

We now focus on the experimental results obtained when the melt composition and the pattern period are changed. We first consider the cases where $L_S \simeq L_0$. In the pure diblock, particles are found only in the middle of the PS domain and form a single line of rather evenly spaced particles (Figure 7c). In blend 2, particles are found throughout the domain, forming a disordered array (Figure 7d). By choosing $L_S > L_0$, one can induce a stretching of the lamellae. In the blends, the effect of stretching is to further broaden the distribution of particles. A different phenomenon occurs in the diblock, where particles aggregate into clusters, still located in the middle of the domain. To characterize the distribution of particles in a quantitative manner, we have measured the average density profiles of particles within a domain. Specifically, Figure 11 shows the probability $\rho_{Pcore}(x)$ that the position x is occupied by the solid core of a particle. Also shown are the density profiles predicted by simulations for $\Lambda_{PA}N = 0$ and $L_S/L_0 = 1$, 1.1, and 1.2.

In general, the theoretical curves appear slightly narrower than those obtained in experiments, but they otherwise reproduce the observed behavior reasonably well: upon increasing the volume fraction of homopolymer or the amount of stretching, the density profiles evolve from a single-peaked curve to a bimodal distribution. Note that even for the highest degree of stretching simulations do not provide any evidence of particle clustering. The experimentally observed aggregation for the stretched pure diblock probably depends on the details of the interaction between particles and possibly on some direct (not polymer-mediated) interactions between particles. We have not attempted to include such interactions in our coarse grain model. As shown in Figure 6, a particle which has a neutral interaction with the surrounding polymer induces in its vicinity a slight decrease in density; the corresponding free energy penalty is minimized when the particle is located in a region of maximum density, which occurs at a short distance d from the domain interface. On the other hand, the strong repulsion for B beads drives the particles away from the interface. The balance between those two opposite effects yields an optimal location at a fixed distance $d' > d$ from the domain interface, which results in a double-peaked profile only when the domain is wide enough. Note also that the particle distribution does not coincide with other factors such as distribution of homopolymer (or chain ends).

As a stringent test of the validity of our model, we conclude this section by considering a pattern that compresses and stretches the copolymer domains in an inhomogeneous manner and by examining the local distribution of nanoparticles throughout a relatively large sample. More specifically, we examine a pattern consisting of an array of lines bent at a right angle (Figure 12). Using a blend, rather than a diblock, allows for a perfect replication of the underlying substrate by the copolymer lamellae. As previously found,[53] the corners of the bends are enriched in homopolymer, while their immediate

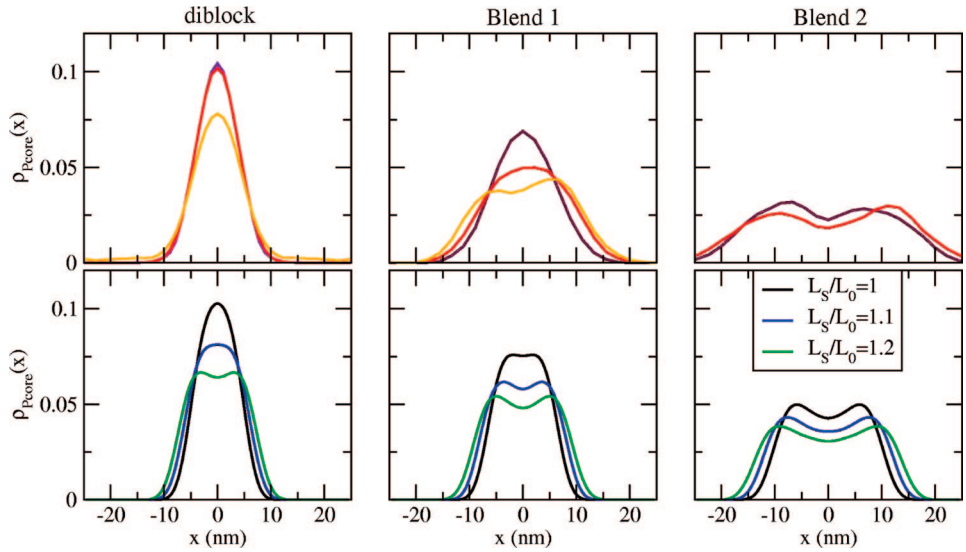

Figure 11. Effect of a pattern-induced stretching of the lamellae on the distribution of particle cores. $\rho_{Pcore}(x)$ is the (normalized) probability to find position x occupied by a particle core. Abscissa is expressed in real units. The origin $x = 0$ is taken in the middle of the PS domain. (bottom row) Simulations results. The ratio L_S/L_0 is given in the legend. (top row) Experimental results. L_S/L_0 varies in each case: for the diblock, $L_S/L_0 =$ 1.07, 1.12, 1.22 (from top to bottom); for blend 1, $L_S/L_0 =$ 1.02, 1.11, 1.20; and for blend 2, $L_S/L_0 =$ 0.99, 1.06.

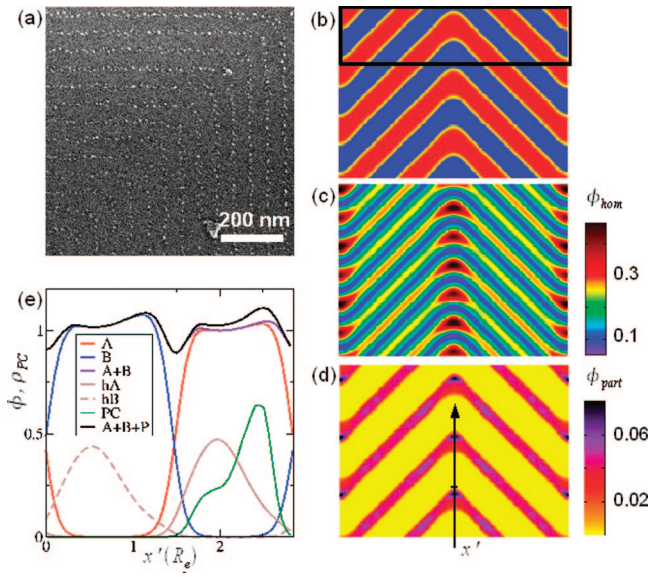

Figure 12. Thin film of blend 1 and particles laid over a substrate patterned with stripes bent at right angle. (a) Top-down SEM image of the experimental system ($L_S/L_0 = 1.02$). (b−e) Simulation result. The simulated system has been replicated three times for clarity. All colormaps (b−d) show quantities averaged over the thickness of the film. (b) The A and B domains are shown in red and blue respectively; they replicate the underlying pattern. (c) Volume fraction of homopolymer. (d) Volume fraction of particle. (e) Distribution of particle center (PC) and density profiles at the corner, along the x'-axis shown in (d). The legend is similar to that of Figure 10, while the black curve (A + B + P) is the total density of the system (polymer and particle).

vicinity is slightly depleted in homopolymer. As shown in Figure 12e, the homopolymer chains segregate to the inner half of the bend, whereas the particles are found preferentially at the outer edge of the bend, where the polymer density reaches a maximum. This behavior is not clearly visible in the experimental images, where the particles tend to form slightly rounded bends. The micrographs taken before the polymer was removed, however, do suggest that the theoretically predicted concentration of nanoparticles in the outer edges of the corners is indeed plausible. More generally, the model is able to reproduce most of the experimental behavior as captured by the distribution of particles, including the effect of changing the homopolymer volume fraction and inducing a stretching of the lamellae through the substrate pattern.

V. Conclusion

A coarse grain model has been presented for study of dense block copolymers melts and particle filled polymers. In contrast to SCFT, it is a particle-based method where the local densities are defined from the bead positions through a smoothing procedure. The influence of the discretization parameters has been examined in detail, for parameters that are representative of a typical PS−PMMA block copolymer melt. In the vicinity of a substrate (or impenetrable object), a high discretization is required to obtain accurate results. For interfaces between domains, a moderate discretization is appropriate.

While we have only discussed MC simulations in their most basic implementation, there is a whole array of MC techniques that could be applied within the general framework of our model. Such techniques could facilitate sampling and further expand the usefulness of our proposed approach. Note that, in contrast to models where hard-core potentials forbid beads from overlapping, our chains can cross each other; as a consequence, moving entire chains is not as demanding as it is in atomistic simulations. In order to generate a perfectly ordered morphology, it is highly advantageous to use concerted moves that involve a large number of chains. Accordingly, it would be useful to explore the efficacy of various available collective moves proposed in the literature.

We have considered Gaussian chains and the standard form for the nonbonded interaction in a dense, compressible melt. However, in contrast to SCFT, it would be straightforward to consider other kinds of bonded interactions or nonbonded interactions (as long as they depend on the local densities only). An other attractive feature of the method is the simplicity of implementation, in particular when using the PM_0 discretization scheme.

There are at least three directions in which to further develop our proposed approach. First, efficient numerical methods for computing the free energy should be developed.[54] Second, we have considered equilibrium properties of dense melts for which the interdigitation number $\sqrt{N}$ is high and fluctuation effects are not expected to be significant. It remains to be seen whether

our method can faithfully capture fluctuation effects when they become important. Finally, it would be useful to take into account entanglement effects so as to give a physically realistic description of the dynamics.

Acknowledgment. Support was provided by the Semiconductor Research Corporation, the NSF UW Nanoscale Science and Engineering Center (DMR-0425880), and the Volkswagen Foundation. This work used the facilities and staff at the UW Synchrotron Radiation Center (NSF DMR-0084402), UW Center for Nanotechnology, the computational resources provided by GLOW, and the John von Neumann-Institute for Computing, Jülich, Germany.

References and Notes

(1) Fredrickson, G. *The Equilibrium Theory of Inhomogeneous Polymers*; Clarendon Press: Oxford, 2006.
(2) Matsen, M. W.; Schick, M. *Phys. Rev. Lett.* **1994**, *72*, 2660.
(3) Fredrickson, G. H.; Ganesan, V.; Drolet, F. *Macromolecules* **2002**, *35*, 16.
(4) Alexander-Katz, A.; Moreira, A. G.; Fredrickson, G. H. *J. Chem. Phys.* **2003**, *118*, 9030.
(5) Alexander-Katz, A.; Moreira, A. G.; Sides, S. W.; Fredrickson, G. H. *J. Chem. Phys.* **2005**, *122*, 8.
(6) Alexander-Katz, A.; Fredrickson, G. H. *Macromolecules* **2007**, *40*, 4075.
(7) Binder, K. *Monte Carlo and Molecular Dynamics Simulations in Polymer Science*; Oxford University Press: New York, 1995.
(8) Baschnagel, J.; Binder, K.; Doruker, P.; Gusev, A. A.; Hahn, O.; Kremer, K.; Mattice, W. L.; Muller-Plathe, F.; Murat, M.; Paul, W.; Santos, S.; Suter, U. W.; Tries, V. *Adv. Polym. Sci.* **2000**, *152*, 41.
(9) Daoulas, K. C.; Müller, M.; de Pablo, J. J.; Nealey, P. F.; Smith, G. D. *Soft Matter* **2006**, *2*, 573.
(10) Daoulas, K. C.; Müller, M. *J. Chem. Phys.* **2006**, *125*, 184904.
(11) Daoulas, K. C.; Müller, M.; Stoykovich, M. P.; Park, S. M.; Papakonstantopoulos, Y. J.; de Pablo, J. J.; Nealey, P. F.; Solak, H. H. *Phys. Rev. Lett.* **2006**, *96*, 036104.
(12) Müller, M.; Smith, G. D. *J. Polym. Sci., Part B: Polym. Phys.* **2005**, *43*, 934.
(13) Laradji, M.; Guo, H.; Zuckermann, M. *J. Phys. Rev. E* **1994**, *49*, 3199.
(14) Soga, K. G.; Guo, H.; Zuckermann, M. *J. Europhys. Lett.* **1995**, *29*, 531.
(15) Soga, K. G.; Zuckermann, M. J.; Guo, H. *Macromolecules* **1996**, *29*, 1998.
(16) Balazs, A. C.; Emrick, T.; Russell, T. P. *Science* **2006**, *314*, 1107.
(17) Mackay, M. E.; Tuteja, A.; Duxbury, P. M.; Hawker, C. J.; Van Horn, B.; Guan, Z. B.; Chen, G. H.; Krishnan, R. S. *Science* **2006**, *311*, 1740.
(18) Bockstaller, M. R.; Mickiewicz, R. A.; Thomas, E. L. *Adv. Mater.* **2005**, *17*, 1331.
(19) Kim, B. J.; Fredrickson, G. H.; Hawker, C. J.; Kramer, E. J. *Langmuir* **2007**, *23*, 7804.
(20) Reister, E.; Fredrickson, G. H. *J. Chem. Phys.* **2005**, *123*, 214903.
(21) Milner, S. T. *Science* **1991**, *251*, 905.
(22) Bockstaller, M. R.; Lapetnikov, Y.; Margel, S.; Thomas, E. L. *J. Am. Chem. Soc.* **2003**, *125*, 5276.
(23) Chiu, J. J.; Kim, B. J.; Kramer, E. J.; Pine, D. J. *J. Am. Chem. Soc.* **2005**, *127*, 5036.
(24) Kim, B. J.; Chiu, J. J.; Yi, G. R.; Pine, D. J.; Kramer, E. J. *Adv. Mater.* **2005**, *17*, 2618.
(25) Lin, Y.; Boker, A.; He, J. B.; Sill, K.; Xiang, H. Q.; Abetz, C.; Li, X. F.; Wang, J.; Emrick, T.; Long, S.; Wang, Q.; Balazs, A.; Russell, T. P. *Nature* **2005**, *434*, 55.
(26) Thompson, R. B.; Ginzburg, V. V.; Matsen, M. W.; Balazs, A. C. *Science* **2001**, *292*, 2469.
(27) Lee, J. Y.; Shou, Z.; Balazs, A. C. *Phys. Rev. Lett.* **2003**, *91*, 136103.
(28) Lee, J. Y.; Thompson, R. B.; Jasnow, D.; Balazs, A. C. *Macromolecules* **2002**, *35*, 4855.
(29) Thompson, R. B.; Lee, J. Y.; Jasnow, D.; Balazs, A. C. *Phys. Rev. E* **2002**, *66*, 7.
(30) Lee, J. Y.; Thompson, R. B.; Jasnow, D.; Balazs, A. C. *Phys. Rev. Lett.* **2002**, *89*, 155503.
(31) Sides, S. W.; Kim, B. J.; Kramer, E. J.; Fredrickson, G. H. *Phys. Rev. Lett.* **2006**, *96*, 250601.
(32) Helfand, E.; Tagami, Y. *J. Chem. Phys.* **1972**, *56*, 3592.
(33) Hockney, R. W.; Eastwood, J. W. *Computer Simulation Using Particles*; IOP: Bristol, 1988.
(34) Deserno, M.; Holm, C. *J. Chem. Phys.* **1998**, *109*, 7678.
(35) Klapp, S. H. L.; Diestler, D. J.; Schoen, M. *J. Phys.: Condens. Matter* **2004**, *16*, 7331.
(36) Hoogerbrugge, P. J.; Koelman, J. *Europhys. Lett.* **1992**, *19*, 155.
(37) Koelman, J.; Hoogerbrugge, P. J. *Europhys. Lett.* **1993**, *21*, 363.
(38) Espanol, P.; Warren, P. *Europhys. Lett.* **1995**, *30*, 191.
(39) Groot, R. D.; Warren, P. B. *J. Chem. Phys.* **1997**, *107*, 4423.
(40) Eurich, F.; Maass, P. *J. Chem. Phys.* **2001**, *114*, 7655.
(41) Murat, M.; Kremer, K. *J. Chem. Phys.* **1998**, *108*, 4340.
(42) Doi, M.; Edwards, S. *The Theory of Polymer Dynamics*; University Press: Oxford, 1986.
(43) Parrinello, M.; Rahman, A. *J. Appl. Phys.* **1981**, *52*, 7182.
(44) Ray, J. R.; Rahman, A. *J. Chem. Phys.* **1984**, *80*, 4423.
(45) Tyler, C. A.; Morse, D. C. *Macromolecules* **2003**, *36*, 8184.
(46) Barrat, J. L.; Fredrickson, G. H.; Sides, S. W. *J. Phys. Chem. B* **2005**, *109*, 6694.
(47) Detcheverry, F. A.; Daoulas, K. C.; Müller, M.; de Pablo, J. J., to appear in *Coarse-graining of condensed phase and biomolecular systems*; Voth, G., Ed.
(48) Kang, H.; Detcheverry, F. A.; Mangham, A. N.; Stoykovich, M. P.; Daoulas, K. C.; Hamers, R. J.; Müller, M.; de Pablo, J. J.; Nealey, P. F. *Phys. Rev. Lett.* **2008**, *100*, 148303.
(49) Wang, Q.; Nealey, P. F.; de Pablo, J. J. *J. Chem. Phys.* **2003**, *118*, 11278.
(50) Schultz, A. J.; Hall, C. K.; Genzer, J. *Macromolecules* **2005**, *38*, 3007.
(51) Buxton, G. A.; Lee, J. Y.; Balazs, A. C. *Macromolecules* **2003**, *36*, 9631.
(52) Pryamitsyn, V.; Ganesan, V. *Macromolecules* **2006**, *39*, 8499.
(53) Stoykovich, M. P.; Müller, M.; Kim, S. O.; Solak, H. H.; Edwards, E. W.; de Pablo, J. J.; Nealey, P. F. *Science* **2005**, *308*, 1442.
(54) Müller, M.; Daoulas, K. C. *J. Chem. Phys.* **2008**, *128*, 024903.
(55) Pickett, G. T.; Balazs, A. C. *Macromolecules* **1997**, *30*, 3097.
(56) Wang, Q.; Yan, Q. L.; Nealey, P. F.; de Pablo, J. J. *J. Chem. Phys.* **2000**, *112*, 450.
(57) Indeed, we have observed that using ΔL too small, microphase separation does not occur in a diblock, even at high χN.
(58) We neglect the difference between the theoretical value of R_e for an isolated, non-interacting chain and the value measured in MC simulations of a homopolymer melt because they are usually close to each other (see ref 10).
(59) Since the curves in Figure 2 result from an average over the y and z directions, the density in the center of the cell is actually higher than the maximum in $\phi(x)$.
(60) Averaged density profiles have been computed with N ranging from to 32 to 2048 and ΔL ranging from 0.16 to 0.04 R_e. The corresponding n_{int}, given by $n_{cell} = \rho_0 \Delta L^3$ with the PM_0 scheme and $8n_{cell}$ with the PM_1 scheme, spans the approximate range $1-10^2$. On the one hand, we have observed that the largest value of induces some artifacts, such as oscillations in the density profile near a hard wall. On the other hand, $n_{cell} \lesssim 1$ prevents phase separation in the diblock. Accordingly, we choose n_{int} in the range $10-50$, where the particular value has a weak or negligible influence.
(61) The lamellar spacings in the bulk and in a thin film are found to be the same (within the error bars), as was observed in SCFT[55] and MC simulations on a lattice.[56]
(62) In a thin film, the local densities depend not only on x but also on the z coordinate. In particular, in the case of the blend, the distribution of homopolymer is not homogeneous across the thickness of the film.[53] However, for simplicity, we compare the average density profiles in the x direction rather than the two-dimensional density $\phi_A(x,z)$.

MA702514V